Functionalization of Poly(oligo(ethylene glycol) methacrylate) Films on Gold and Si/SiO_2 for Immobilization of Proteins and Cells: SPR and QCM Studies

Bong Soo Lee,[†] Young Shik Chi,[†] Kyung-Bok Lee,[‡] Yang-Gyun Kim,[§] and Insung S. Choi*,[†]

Department of Chemistry and School of Molecular Science (BK21), Center for Molecular Design and Synthesis, KAIST, Daejeon 305-701, Korea, Glycomics Team, Korea Basic Science Institute (KBSI), Daejeon 305-333, Korea, and Department of Chemistry, School of Natural Sciences, Sungkyunkwan University, Suwon 440-746, Korea

Received August 13, 2007; Revised Manuscript Received October 8, 2007

Thin films of a biocompatible and nonbiofouling poly(oligo(ethylene glycol) methacrylate) (*p*OEGMA) with various thicknesses were formed on gold and Si/SiO_2 substrates by a combination of the formation of self-assembled monolayers (SAMs) terminating in bromoester—an initiator of atom transfer radical polymerization (ATRP)—and surface-initiated ATRP. After the formation of the *p*OEGMA films, terminal hydroxyl groups of side chains divergent from the methacrylate backbones were activated with *N*,*N*′-disuccinimidyl carbonate (DSC), and the DSC-activated *p*OEGMA films were reacted with (+)-biotinyl-3,6,9-trioxaundecanediamine (Biotin-NH_2) to form biotinylated *p*OEGMA films. By surface plasmon resonance experiments with the target protein (streptavidin) and model proteins (fibrinogen and lysozyme), we verified that the resulting films showed the enhanced signal-to-noise ratio (~10-fold enhancement) for the biospecific binding of streptavidin compared with the biotinylated substrate prepared from carboxylic acid-terminated SAMs. Quartz crystal microbalance measurements were also carried out to obtain the surface coverage of streptavidin and fibrinogen adsorbed onto the biotinylated *p*OEGMA films with various thicknesses and to investigate the effect of film thicknesses on the biospecific binding of streptavidin. Both the binding capacity of streptavidin and the signal-to-noise ratio of streptavidin/fibrinogen were found to be saturated at the 20 nm thick *p*OEGMA film. In addition, to demonstrate a wide applicability of the *p*OEGMA films, we constructed micropatterns of streptavidin and cells by microcontact-printing biotin-NH_2 and poly-L-lysine onto the DSC-activated *p*OEGMA films, respectively.

Introduction

In recent years, there has been a great deal of interest in the development of biodevices, such as biosensors or microarrays, which recognize biospecific interactions, such as DNA hybridization, and peptide-antibody and protein–protein interactions at interfaces.[1–6] It is an important issue for the efficient operation of biodevices to maximize the specific binding of targets and minimize any nonspecific binding simultaneously. As a result, there have been various efforts to construct 2- or 3-dimensional (2- or 3-D) platforms that meet the desired characteristics with molecular-level control.

In the aspect of the minimization of any nonspecific binding, a number of studies on materials, such as polysaccharides,[7] dextran,[8] cellulose dialysis membranes,[9] zwitterionic compounds,[10–16] and poly(ethylene glycol) (PEG),[17–28] have pursued the elimination/minimization of the unwanted, nonspecific adhesion of biological entities. In particular, PEG has extensively been investigated as a material with significant inertness to cell and protein adhesion, good biocompatibility, low toxicity, nonimmunogenicity, and high water solubility.[29,30] Various methods have been developed for the introduction of ethylene glycol (EG) onto surfaces, exemplified by the formation of self-assembled monolayers (SAMs),[17–19] covalent grafting,[21–26] and physisorption.[27,28] Although the reported methods were successful in the introduction of nonbiofouling EG groups onto surfaces, these systems generally showed a limited binding capacity of target biomaterials because of the intrinsic 2-D structure of organic thin films, such as SAMs, or difficulty in the introduction of a number of reactive functional groups even onto semi-3-D polymeric films.[19,26] In this point of view, the carboxymethylated dextran chip (CM5 chip) for surface plasmon resonance (SPR) experiments would be a good model for ideal bioplatforms because dextran is relatively nonbiofouling and the functionalized dextran bears a number of reactive caboxylate groups that can be used for the immolization of small molecules and biomolecules.[19,31] As a related work, Bruening and co-workers recently reported that the high-capacity binding of proteins onto surfaces could be achieved by the derivatization of carboxylic acid groups of poly(acrylic acid) brushes.[32]

Among the coating materials composed of EG groups, poly(oligo(ethylene glycol) methyl ether methacrylate) (*p*OEGMEMA), developed by Chilkoti and co-workers, has some advantages over other EG-based materials.[22–24] The grafted *p*OEGMEMA is composed of a number of oligo(ethylene glycol) side chains divergent from the polymer backbone of methacrylate groups. Although the terminal groups of OEGME were nonreactive methoxy groups in their studies, *p*OEGMEMA-based films would have been efficient bioplatforms with high binding capacity if the terminal methoxy groups had been replaced with any reactive functional groups. As a functional

* Corresponding author. E-mail: ischoi@kaist.ac.kr.
† Department of Chemistry and School of Molecular Science (BK21), Center for Molecular Design and Synthesis, KAIST.
‡ Glycomics Team, Korea Basic Science Institute.
§ Department of Chemistry, School of Natural Sciences, Sungkyunkwan University.

10.1021/bm7009043 CCC: $37.00
Published on Web 11/27/2007

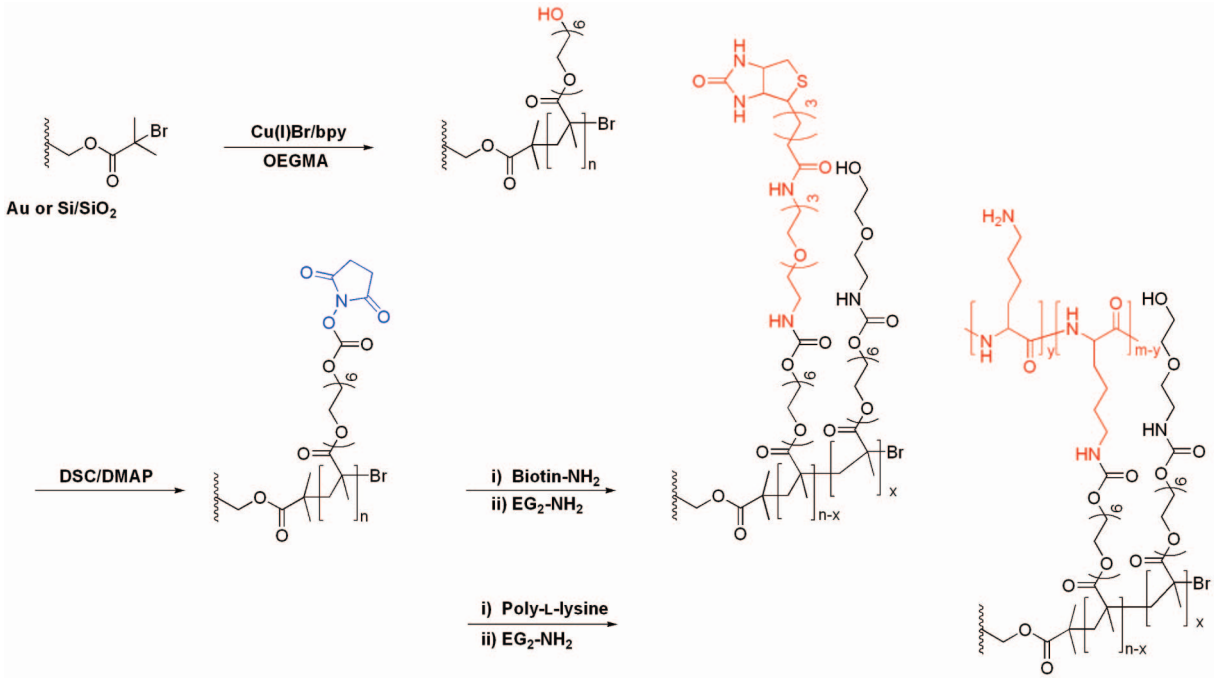

Figure 1. Schematic representation of the procedure.

derivative of *p*OEGMEMA, poly(oligo(ethylene glycol) methacrylate) (*p*OEGMA), presenting the terminal hydroxyl group of OEG, was also grown from surfaces by surface-initiated polymerization. The hydroxyl group was utilized for the orientation-controlled attachment of proteins through multistep, biochemical processes by Klok and co-workers.[25] Anseth and co-workers reported that antibody-modified, acrylated PEG monomers could be used to form an antibody-attached polymeric film for the enhanced detection of antigens.[33] Recently, Collard and co-workers reported the direct attachment of peptides onto the *p*OEGMA films on Ti for enhancing the biological performance of Ti-based orthopedic and dental devices.[34]

We have previously reported that the terminal bromide group of the *p*OEGMEMA backbone could be used for the selective immobilization of biomolecules via click chemisty,[26] where a single molecule of interest was coupled with one *p*OEGMEMA chain. During the study, we realized that the maximized functionalizability would be favorable for a biospecific binding in some cases and the binding specificity/capacity depended upon the thickness of polymeric layers. The purpose of this work was 2-fold: (1) to develop a simple but versatile method for multiply functionalizing OEG-based polymer films, and (2) to investigate the effect of polymer thickness on the binding capacity and signal-to-noise (*S*/*N*) ratios for target and model proteins. Specifically, intact *p*OEGMA films were grown from gold and Si/SiO_2 substrates with different thicknesses, and the hydroxyl group of OEG was activated with *N,N*′-disuccinimidyl carbonate (DSC) and an amide coupling reaction was utilized for the immobilization of biomolecules. To demonstrate the feasibility of the DSC-based activation, micropatterns of proteins and cells were generated.

Experimental Section

Materials. Absolute ethanol (EtOH, 99.9+%, Merck), absolute methanol (MeOH, 99.9+%, Merck), anhydrous *N,N*′-dimethylformamide (DMF, 99.8+%, Aldrich), toluene (J. T. Baker), copper(I) bromide (Cu(I)Br, 99.999%, Aldrich), 2,2′-dipyridyl (bpy, 99+%, Aldrich), *N,N*′-disuccinimidyl carbonate (DSC, Aldrich), 4-(dimethylamino)pyridine (DMAP, Fluka), 2-(2-aminoethoxy)ethanol (EG_2-NH_2, 98%, Aldrich), poly-L-lysine (PLL, Sigma), (+)-biotinyl-3,6,9-trioxaundecanediamine (biotin-NH_2, Pierce), *N*-hydroxysuccinimide (NHS, 97%, Aldrich), 1-ethyl-3-(3-dimethylaminopropyl)carbodiimide hydrochloride (EDC, TCI), fibrinogen (Sigma), lysozyme (Sigma), streptavidin (SA, Pierce), and phosphate buffered saline (PBS, Sigma) were used as received. Poly(ethylene glycol) methacrylate (OEGMA, M_n: ~360, Aldrich) was passed through a column of activated, basic aluminum oxide to remove inhibitors. $[BrC(CH_3)_2COO(CH_2)_{11}S]_2$,[35] $BrC(CH_3)_2COO(CH_2)_3SiCl_3$,[36] and $HS(CH_2)_{11}(OCH_2CH_2)_5OCH_2COOH$ (EG5-COOH)[37] were prepared according to the literature.

Preparation of SAMs of ATRP Initiators. The SAMs of ATRP initiators were formed on gold and Si/SiO_2 substrates (Figure 1). Gold substrates were prepared by thermal evaporation of 5 nm of titanium and 100 nm of gold onto silicon wafers. The SAMs of $[BrC(CH_3)_2COO(CH_2)_{11}S]_2$ were prepared by immersing a gold substrate in a 1 mM ethanolic solution of $[BrC(CH_3)_2COO(CH_2)_{11}S]_2$ for 12 h at room temperature. After the formation of the SAMs, the substrates were thoroughly rinsed with ethanol several times and then dried in a stream of argon. Si/SiO_2 substrates (silcon wafers or glass) were cleaned for 2 min in piranha solution (3:7 by volume of 30% H_2O_2 and H_2SO_4; *safety note: the piranha solution reacts violently with organic materials and must be handled with extreme care*). The substrates were then rinsed with H_2O and ethanol and dried under a stream of argon. The substrates were subsequently treated with O_2-plasma and then the plasma-oxidized substrates were immersed in an anhydrous toluene solution (30 mL) containing 10 μL of $[BrC(CH_3)_2COO(CH_2)_3SiCl_3]$ for 10 min at room temperature. After the formation of the SAMs, the substrates were thoroughly rinsed with toluene and ethanol several times and then dried in a stream of argon.

Surface-Initiated ATRP (SI-ATRP) of OEGMA. We used 1 and 2 M OEGMA to obtain *p*OEGMA films with various thicknesses on gold substrates. To a Schlenk tube containing deionized water (degassed, 1.34 mL) and methanol (degassed, 5.39 mL) were added Cu(I)Br (143 mg, 1 mmol), bpy (312 mg, 2 mmol), and OEGMA (3.26 mL, 10 mmol). The final concentration of OEGMA was 1 M. In addition, 2 M OEGMA was used (0.70 mL of H_2O, 2.78 mL of MeOH, 2 mmol of Cu(I)Br, and 4 mmol of bpy and 20 mmol of OEGMA). The resulting dark-red solution was bubbled with Ar gas for 10 min. SI-ATRP was initiated by transferring the mixture to a degassed Schlenk tube th

contained a gold substrate presenting ATRP initiators, and then the mixture was soaked for a specified time (3–1200 min) under argon at room temperature. The polymerization was terminated by exposing the reaction to air and pouring water into the Schlenk tube. The termination step caused the reaction solution to turn blue, indicating the oxidation of Cu(I) to Cu(II). For Si/SiO_2 substrates, 1 M OEGMA was used with platforms for generating micropatterns of proteins and cells. All the *p*OEGMA-coated substrates were thoroughly washed with deionized water and methanol in order to remove any physisorbed polymers and then dried in a stream of argon.

Activation of *p*OEGMA Films with *N,N′*-Disuccinimidyl Carbonate (DSC) and Subsequent Coupling of Biotin-NH_2. To activate terminal hydroxyl groups of side chains in the *p*OEGMA films, the films were immersed in dry DMF solution containing 0.1 M DSC and 0.1 M DMAP for 14 h at room temperature under an argon atmosphere.[38] The resulting substrates were rinsed with DMF and CH_2Cl_2 and then dried in a stream of argon.

The DSC-activated *p*OEGMA films were soaked in an ethanolic solution of biotin-NH_2 (1 mg/mL) for 2 h at room temperature. After the reaction, the substrates were washed with ethanol and dried in a stream of argon. Subsequently, to deactivate the unreacted NHS carbonate ester groups, the substrates were immersed in an ethanolic solution of EG_2-NH_2 (0.1 mg/mL) for 1 h at room temperature. After treating with the blocking agent, the substrates were rinsed with ethanol and dried in a stream of argon.

Surface Plasmon Resonance (SPR) Study. SPR measurements were performed with a Biacore instrument (model: Biacore X) to investigate the specific binding capacity of a target protein and nonspecific binding of model proteins onto the biotin-presenting, *p*OEGMA films. The SI-ATRP and biotinylation were performed on a gold substrate (0.8×1.0 cm^2) (D.I. Biotech Ltd., Korea) that had been prepared for the SPR study by a sequential deposition of titanium (1.5 nm) and gold (39 nm) onto a glass cover slip (0.2 nm, no. 2. Corning, reflective index = 1.52). The SPR studies on the specific binding of streptavidin (SA, 0.1 mg/mL) and the nonspecific binding of model proteins (1 mg/mL), such as fibrinogen and lysozyme, were carried out by one injection of 20 μL of a protein solution with a constant flow of the solution (5 μL/min). After the elution of the protein solution for 4 min, the surface was washed with a constant flow rate of the PBS buffer solution (5 μL/min). Protein binding resulted in a shift in the resonance angle that was reported in resonance units (RU; 10000 RU = 1.0°).[39]

As a control experiment, we prepared a biotinylated substrate with the SAMs of EG5-COOH by activation of the carboxylic acid group with EDC and NHS and the subsequent coupling with biotin-NH_2. The carboxylic acid-terminated SAMs (COOH-SAMs) were prepared by immersing a cleaned gold substrate in a 1 mM ethanolic solution of EG5-COOH for 12 h at room temperature. The COOH-SAMs were activated by immersing in an aqueous solution of 75 mM EDC and 15 mM NHS. The biotinylated SAMs were then formed through the reaction of the NHS-activated substrates with an ethanolic solution of biotin-NH_2(1 mg/mL) and the subsequent passivation of the remaining NHS carbonate ester groups by soaking the substrates in an ethanolic solution of EG_2-NH_2 (0.1 mg/mL) for 1 h at room temperature. After the processes, the substrates were thoroughly rinsed with the solvents used for the reaction several times and then dried in a stream of argon.

Quartz Crystal Microbalance (QCM) Study. QCM is an electroacoustic method suitable for mass and viscoelastic analysis of adsorbed layers at the solid/liquid interface.[40–42] Sauerbrey[43,44] provided the description and experimental verification of the mass/frequency relationship between rigid foreign layers firmly attached to the quartz crystal resonators. The frequency changes are directly proportional to the added mass as long as the added mass behaves elastically similarly to the quartz itself as the equation shown below:

$$\Delta m = -C\Delta f/n$$

where Δf is the change in the resonance frequency due to the added mass (Δm), and C is a proportionality constant (17.7 ng/cm^2·Hz for a 5 MHz quartz crystal),[41] which depends only on the intrinsic properties of the quartz.

To quantify the biospecific binding of SA and the nonspecific binding of fibrinogen, the QCM measurements were performed using a Q-sense E4 system (Q-sense AB). The QCM sensor consisted of a disk-shaped, AT-cut piezoelectric quartz crystal, coated with metallic electrodes on both sides. The QCM sensor crystal operated at a frequency of 4.95 MHz ± 50 kHz. Gold-coated quartz crystals were coated with the biotinylated *p*OEGMA films with various thicknesses by following the procedure mentioned above. The thicknesses of the *p*OEGMA films were 3, 8, 20, 31, and 46 nm. For the QCM measurements, the *p*OEGMA-coated crystals were mounted at room temperature, and the stable baseline on the films was confirmed during the prewashing step with PBS buffer (flow rate: 100 μL/min). The adsorption of streptavidin (0.1 mg/mL) or fibrinogen (1 mg/mL) was conducted by injecting a protein solution onto the *p*OEGMA-coated crystal with the flow rate of 100 μL/min for ~18 min and changing the solution to PBS buffer. Time-course changes in the resonant frequency (Δf) were measured simultaneously at the fundamental resonant frequency and six different overtones.

Protein and Cell Patterning by Microcontact Printing (μCP). PDMS stamps were prepared according to the literature method using Sylgard 184 silicone elastomer (Dow Corning).[45] Briefly, a cleaned silicon wafer was spin-coated with a negative photoresist (SU8-50, MicroChem) and processed by photolithography to develop patterns on the surface of the wafer (a master). Subsequently, the master was silanized by (tridecafluoro-1,1,2,2,-tetrahydrooctyl)trichlorosilane under vacuum for 2 h. To cast the PDMS stamp, the master was covered in a petri dish with PDMS oligomers. After curing for 6 h at 60 °C, the PDMS stamp was peeled off from the master. Before use, the PDMS stamp was cleaned and oxidized by an oxygen plasma cleaner (Harrick PDC-002 at medium setting) for 1 min. For the pattern generation of biotin-NH_2 or PLL, the PDMS stamp was inked by spin-casting with an ethanolic solution of biotin-NH_2 (1 mg/mL) or PLL in distilled water (1 mg/mL). The inked stamp was brought into contact with the DSC-activated *p*OEGMA film for 60 s. The stamp was carefully peeled off and then immersed immediately in a solution of EG_2-NH_2 (0.1 mg/mL, 0.1 M sodium bicarbonate) for 1 h and rinsed with distilled water. After the pattern generation of biotin, the sample was immersed in a solution of rodamin (TRITC)-conjugated streptavidin (0.1 mg/mL) in PBS (pH 7.4) at room temperature. After 60 min, the sample was removed, washed several times with PBS and distilled water, and then dried. The micropatterns of streptavidin were characterized by fluorescence microscopy. Chinese hamster ovary cells (CHO-k1), obtained from American Type Culture Collection (ATCC, CCL-61), were grown on tissue culture polystyrene (TCPS) in Ham's F-12 medium supplemented with 25 mM HEPES, 10% (v/v) fetal bovine serum (FBS, Gibco BRL), 100 units/mL penicillin, and 100 mg/ml streptomycin at 37 °C in a humidified atmosphere of 95% air and 5% CO_2. Cells were seeded on the PLL-patterned *p*OEGMA films at a density of 1×10^5 cells/mL. After 1 h, the loosely adhered cells were gently rinsed off with cell culture media and the attached cells were cultured for 12 and 24 h. Patterned cells were stained with a reagent of living cell-staining (CallTracker Green CMFDA, Molecular Probes, Inc.).

Measurements. *(a) Polarized Infrared External Reflectance Spectroscopy (PIERS).* Polarized infrared external reflectance spectroscopy (PIERS) spectra were obtained in a single reflection mode using a dry N_2-purged Thermo Nicolet Nexus FT-IR spectrophotometer equipped with the smart apertured grazing angle (SAGA) accessory. The *p*-polarized light was incident at 80° relative to the surface normal of the substrate, and a narrow band mercury-cadmium-telluride (MCT) detector cooled with liquid nitrogen was used to detect the reflected light. We averaged 4000 scans to yield the spectrum at a resolution of 4 cm^{-1}, and all spectra were reported in the absorption mode relative to a clean gold surface.

(b) Ellipsometry. The thicknesses of the monolayer and polymer films were measured with a Gaertner L116s ellipsometer (Gaertner Scientific

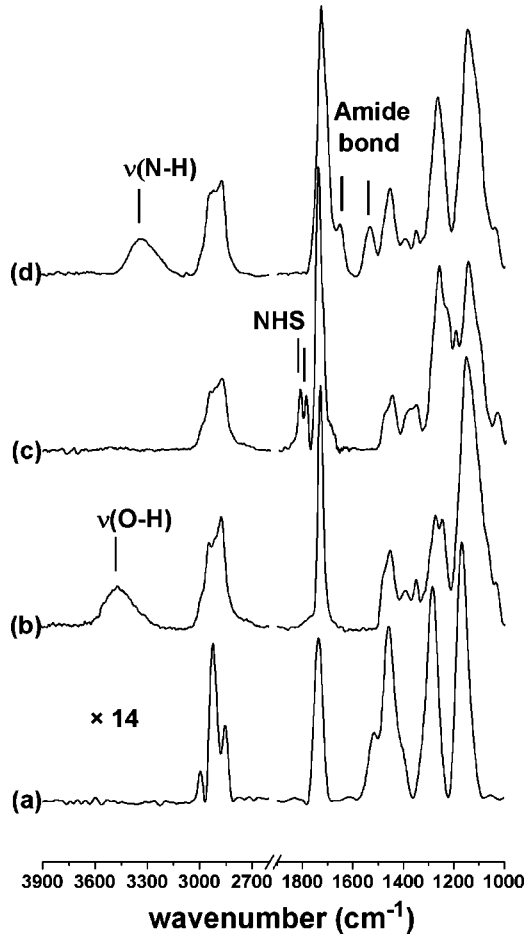

Figure 2. PIERS spectra of the gold substrates: (a) initiator-presenting SAMs, (b) intact *p*OEGMA films, (c) DSC-activated *p*OEGMA films, and (d) biotin-attached *p*OEGMA films.

Corporation, Chicago, IL) equipped with a He-Ne laser (632.8 nm) at a 70° angle of incidence. A refractive index of 1.46 was used for all films.

(c) X-Ray Photoelectron Spectroscopy (XPS). The XPS study was performed with a VG Scientific ESCALAB 250 spectrometer (UK) with monochromatized Al Kα X-ray source. Emitted photoelectrons were detected by a multichannel detector at a take-off angle of 90° relative to the surface. During the measurements, the base pressure was $10^{-9}-10^{-10}$ Torr. Survey spectra were obtained at a resolution of 1 eV from three scans, and high-resolution spectra were acquired at a resolution of 0.05 eV from 5 to 20 scans. All binding energies were determined with the Au 4f7/2 core level peak at 84 eV as a reference.

Results and Discussion

Formation of SAMs and Surface-Initiated ATRP of OEGMA. The SAMs of ATRP initiators, such as $[BrC(CH_3)_2COO(CH_2)_{11}S]_2$ (for gold) and $BrC(CH_3)_2COO(CH_2)_3SiCl_3$ (for Si/SiO_2), were formed by following the reported procedures, and the details were described in the Experimental Section. In the IR spectrum, we observed characteristic peaks of the initiator-presenting SAMs on gold at 2981 and 2853 ($\nu_s(CH_2)$), 2929 ($\nu_{as}(CH_2)$), 1734 ($\nu(C{=}O)$), 1466 ($\nu(-CH_2-)$), and 1171 cm^{-1} ($\nu(C-O)$) (Figure 2a).[26] The ellipsometric thicknesses of the SAMs on gold and Si/SiO_2 were measured to be 14 and 11 Å, respectively. In the wide-scan XPS spectrum of gold substrates, a peak of S 2p was observed at 161.3 eV, indicating the existence of the ATRP initiator (Figure 3a).[23]

The *p*OEGMA films were grown from gold and Si/SiO_2 by surface-initiated ATRP (SI-ATRP) of OEGMA. We varied polymerization time and the concentration of OEGMA to obtain the *p*OEGMA films with various thicknesses on gold. Figure 4 shows the ellipsometric thickness of the resulting *p*OEGMA films as a function of polymerization time. A sigmodial fit (the continuous curve in Figure 4) of the thickness began to be flattened after 20 h of the reaction time. The film thicknesses were obtained from 1 to 180 nm with 2 M OEGMA, and from 1 to 48 nm with 1 M OEGMA, respectively. We characterized the 16 nm thick film on gold as a representative by IR spectroscopy and XPS. The $\nu(O-H)$ peak of the side chain of *p*OEGMA films was observed around 3463 cm^{-1},[46] and a strong band of the carbonyl stretching vibration of the ester group appeared at 1729 cm^{-1}(Figure 2b).[25] In the wide-scan XPS spectrum, the intensity of the Au 4f7/2 peak decreased and that of the O 1s peak increased due to the thickness increase by the polymer formation (Figure 3b). In the high-resolution XPS spectra of carbon 1s regions, we decomposed the carbon peaks from the SAMs and the *p*OEGMA films (Figure 3e,f). The high-resolution carbon peaks of the SAMs were fitted with three unique carbon moieties: $-CH_2-$ (283.6 eV), $-C-O-C-$ (285.0 eV), and $-C{=}O-$ (287.9 eV) (Figure 3e). In contrast to the carbon peaks of the SAMs, the high-resolution carbon peaks of the *p*OEGMA films were fitted with $-CH_2-$ (283.2 eV), $-C-O-C-$ (284.8 eV, the EG groups of the polymeric films), and $-C{=}O-$ (287.3 eV, the carbonyl group of the polymeric films), indicating that the successful formation of *p*OEGMA films (Figure 3f).[24]

Formation of DSC-Activated *p*OEGMA Films and Biotin-Presenting Surfaces. To achieve the covalent attachment of amine-terminated compounds onto the *p*OEGMA films, we used a method of common reactive intermediates, NHS carbonate esters, because the NHS carbonate ester groups were easily coupled with amines, leading to the formation of amide bonds. The *p*OEGMA-presenting substrates were activated to the ones presenting the NHS carbonate ester groups by DSC and DMAP in DMF. After the activation, the ν(O-H) band completely disappeared in the IR spectrum and the two absorption peaks of the symmetric C=O stretching of NHS and the C=O stretching of ester bond newly appeared at 1791 and 1815 cm^{-1}, respectively (Figure 2c).[47] The N 1s peak was observed at 398 eV in the wide-scan XPS spectrum, indicating the successful activation to the NHS carbonate ester groups (Figure 3c).[38]

The biotinylation was performed through the covalent attachment of biotin-NH_2 with the NHS-presenting surface and subsequent treatment of EG_2-NH_2 for passivation of the remaining NHS carbonate ester groups on the *p*OEGMA film. We observed the change of the peaks in the IR spectrum: the ν(N-H) band appeared strongly around 3328 cm^{-1}. In particular, the peaks from the biotin moieties were observed at 1655 (amide I) and 1535 cm^{-1} (amide II) (Figure 2d).[47] In the wide-scan XPS spectrum, the S 2p peak reappeared at 162 eV after the coupling of biotin, indicating the successful immobilization of the biotin-containing compound (Figure 3d).[24]

Nonbiofouling Property of the *p*OEGMA Films: SPR Study. We used SPR spectroscopy to characterize binding specificity/capacity of the *p*OEGMA films on gold and compared the results with that of the COOH-SAMs (as a reference). SPR is an optical technique that is used to monitor localized differences in the reflectivity of incident light from a prism−gold substrate interface caused by the adsorption/desorption of molecules. The SPR technique has shown a great potential for affinity biosensors, allowing real-time analysis of biospeci

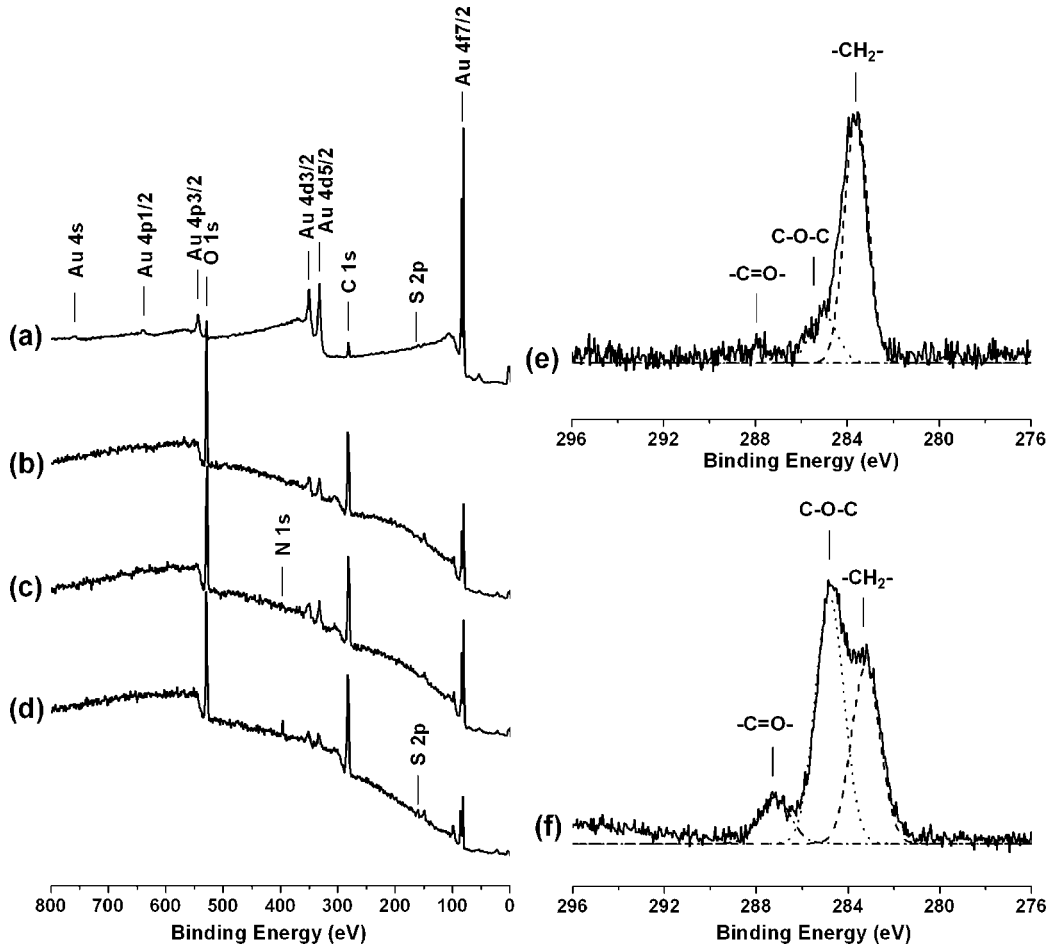

Figure 3. Wide-scan XPS spectra of the gold substrates: (a) initiator-presenting SAMs, (b) intact *p*OEGMA films, (c) DSC-activated *p*OEGMA films, and (d) biotin-attached *p*OEGMA films. High-resolution XPS spectra of C 1s regions acquired from (e) initiator-presenting SAMs and (f) intact *p*OEGMA films.

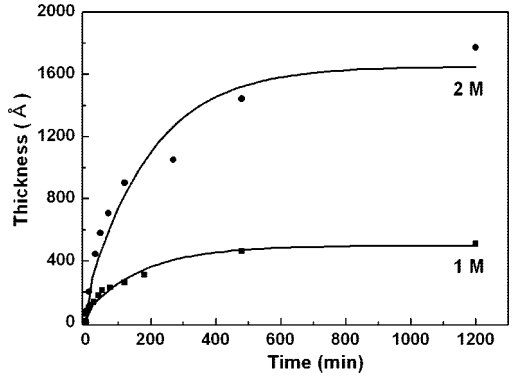

Figure 4. Graph of the ellipsometric thickness of *p*OEGMA films on gold vs polymerization time.

interactions without the use of labeled molecules.[48] In this work, we investigated the binding capacity of streptavidin (SA) onto the biotinylated, 4 nm thick *p*OEGMA film and the biotinylated COOH-SAMs. In addition, nonbiofouling effect of the two biotinylated substrates was tested with fibrinogen and lysozyme (model proteins). Fibrinogen is a large protein that has been known as a "sticky protein", and lysozyme is positively charged under the PBS buffer of pH 7.4.[49]

The binding capacity of SA was measured to be 6485 (648.5 ng/cm^2) and 2556 RU (255.6 ng/cm^2) for the 4 nm thick *p*OEGMA film and the COOH-SAMs, respectively (Figure 5a). These values indicated that the binding capacity of the *p*OEGMA film for SA was about twice than that of the monolayers, and the *p*OEGMA film possessed more biofunctionalizable sites than the 2-D monolayers. In contrast, the trend of nonspecific binding of fibrinogen (29 vs 103 RU) and lysozyme (30 vs 82 RU) was the opposite on the two substrates (Figure 5b). In other words, the introduction of the semi-3-D *p*OEGMA film simultaneously increased the biospecific biotin−streptavidin interactions and decreased the nonspecific adsorption of the model proteins. To quantify the binding properties, we defined the signal-to-noise (*S*/*N*) ratio as the amount of bound SA divided by that of the model proteins, which would indicate the binding specificity of SA onto the biotinylated surfaces (Table 1). The *S*/*N* ratios were calculated to be 223.6 (for the *p*OEGMA film) and 21.8 (for the COOH-SAMs) with fibrinogen as a model protein. With lysozyme, the ratios were 216.2 and 31.2, respectively. We also compared these values with the ones previously obtained from the 4 nm thick *p*OEGMEMA film, where click chemistry was utilized for bioconjugation.[26] We obtained about 10-fold enhancement of the *S*/*N* ratios, compared with both the 4 nm thick *p*OEGMEMA film and the COOH-SAMs. Considering the enhanced *S*/*N* ratios, we believe that the biofunctionalizable, semi-3-D *p*OEGMA film would be effectively utilized for selectively immobilizing biomolecules (DNA, proteins, and cells) and acquiring high detection selectivity.

Saturation of Binding Capacity of *p*OEGMA Films. Several papers have previously addressed some aspects of the quantitative interpretation of SPR signals in terms of adlayer structural parameters. Most of these previous reports addressed the quantitative analysis of adsorbed films that were much

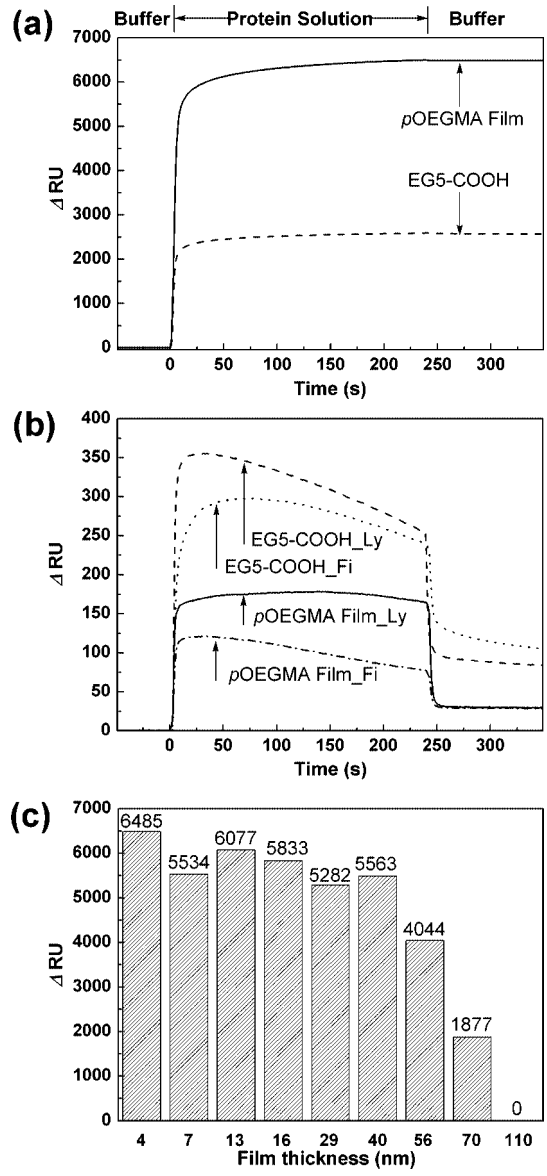

Figure 5. SPR sensorgrams for (a) specific binding of streptavidin (SA), (b) nonspecific binding of fibrinogen (Fi) and lysozyme (Ly) onto the biotinlyated *p*OEGMA film and COOH-SAMs, and (c) thickness-dependent binding capacity of SA measured by SPR.

Table 1. Surface Coverage (SC) and Signal-to-Noise (*S*/*N*) Ratios for Target and Model Proteins Calculated from SPR Data

	substrate					
	4 nm thick *p*OEGMEMA[a]		COOH-SAMs		4 nm thick *p*OEGMA	
	SC (ng/cm^2)	*S*/*N*	SC (ng/cm^2)	*S*/*N*	SC (ng/cm^2)	*S*/*N*
SA	61.8[a]		255.6		648.5	
fibrinogen	3.7[a]	16.7	10.3	21.8	2.9	223.6
lysozyme	4.0[a]	15.5	8.2	31.2	3.0	216.2

[a] Ref 23.

thinner than the decay length of the evanescent field, in the so-called linear-response regime. On the other hand, a few papers have addressed the SPR response to thicker films, beyond the linear regime. For example, Liedberg et al. theoretically showed that the SPR response to local changes in the index of refraction (the shift in resonance angle, $\Delta\Theta_{sp}°$) decayed exponentially with the distances from a metal surface.[39] For example, the $\Delta\Theta_{sp}°$ values at 1 and 250 nm distances were calculated to be about

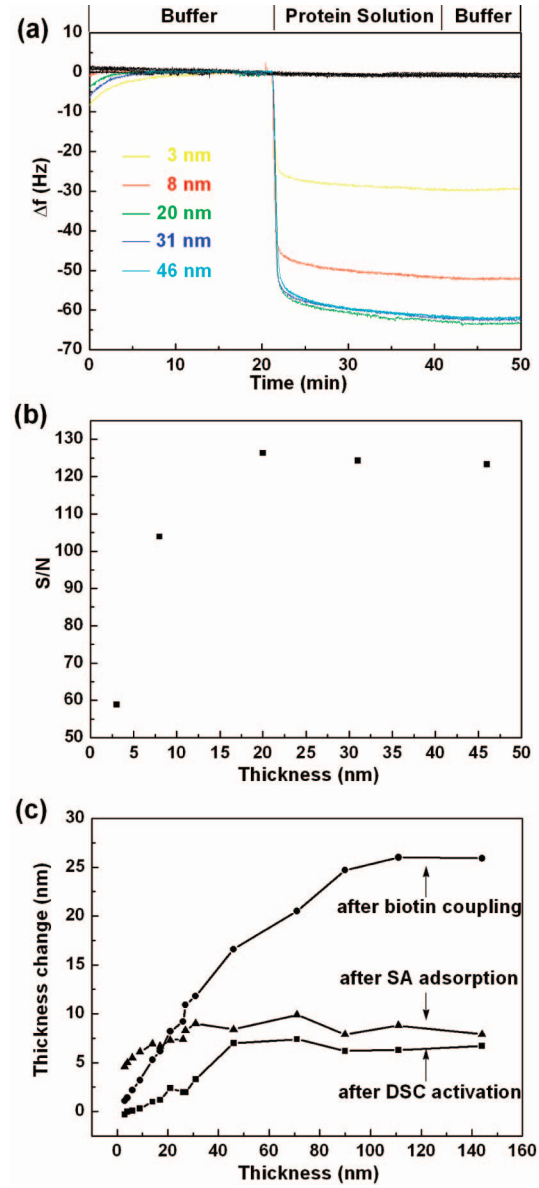

Figure 6. (a) QCM frequency shift of SA (five color lines) and fibrinogen (black line) onto the biotinylated *p*OEGMA films with various thicknesses. (b) Thickness-dependent signal-to-noise ratios (SA/fibrinogen). (c) Ellipsometric thickness changes after DSC activation, biotin coupling, and SA adsorption.

0.5° and 0.05°, respectively. These calculations imply that the binding capacity of biomolecules onto thick films could be underestimated, when thick films are employed. In addition, Lukosz used an approach of perturbation theory on Maxwell's equations to calculate the effective refractive index of uniform adlayers and reported that the value varied linearly with film thicknesses for thin films but showed the increased nonlinearity for thick films.[50] We performed the SPR study for *p*OEGMA films with various thicknesses, such as 4, 7, 13, 16, 29, 40, 56, 70, and 110 nm, and observed that the apparent binding capacity of SA decreased as the thickness of the polymer increased (Figure 5c). For example, the binding capacity of the 70 nm thick *p*OEGMA film was 1877 RU, which was about one-third of that of the 4 nm thick film (6485 RU). In addition, the binding capacity of the 110 nm thick *p*OEGMA film was measured to be 0 RU, no shift in the resonance angle. On the other hand, the ellipsometric measurements showed that the mean thicknesses of the 110 nm thick *p*OEGMA film were increased af

Table 2. Surface Coverage (SC) and Signal-to-Noise (*S*/*N*) Ratios for Streptavidin (SA) and Fibrinogen (Fi) onto the Biotinylated *p*OEGMA Films with Various Thicknesses Calculated by QCM Data

	thickness									
	3 nm		8 nm		20 nm		31 nm		46 nm	
	SC (ng/cm^2)	*S*/*N*	SC (ng/cm^2)	*S*/*N*	SC (ng/cm^2)	*S*/*N*	SC (ng/cm^2)	*S*/*N*	SC (ng/cm^2)	*S*/*N*
SA	523.9		924.9		1124.0		1106.3		1097.4	
Fi	8.9	58.9	8.9	103.9	8.9	126.3	8.9	124.3	8.9	123.3

functionalizations and binding of SA: the thickenesses of the DSC-activated, biotinylated, and SA-bound films were 117, 143, and 152 nm, respectively. The observed $\Delta\Theta_{sp}°$ value of zero was not in agreement with the adsorption of SA (the 9 nm thickness increase). On the basis of the results, we thought that the SPR response was deviated from the linear-response regime, as the thickness of the *p*OEGMA films was increased, and the SPR technique might not be suitable for investigating the effect of film thicknesses on the binding capacity of thick films.[51]

As a complimentary method, we used QCM to investigate the binding characteristics of proteins onto the biotinylated *p*OEGMA films with various thicknesses. The QCM measurements were performed with various overtones (see the Supporting Information), and we used the QCM frequency shift measured at the overtone of $n = 9$ as a representative to compare the binding capacity of SA (the target protein) and fibrinogen (a model protein) (Figure 6a and Table 2). The thicknesses of the films used were 3, 8, 20, 31, and 46 nm. First, we measured

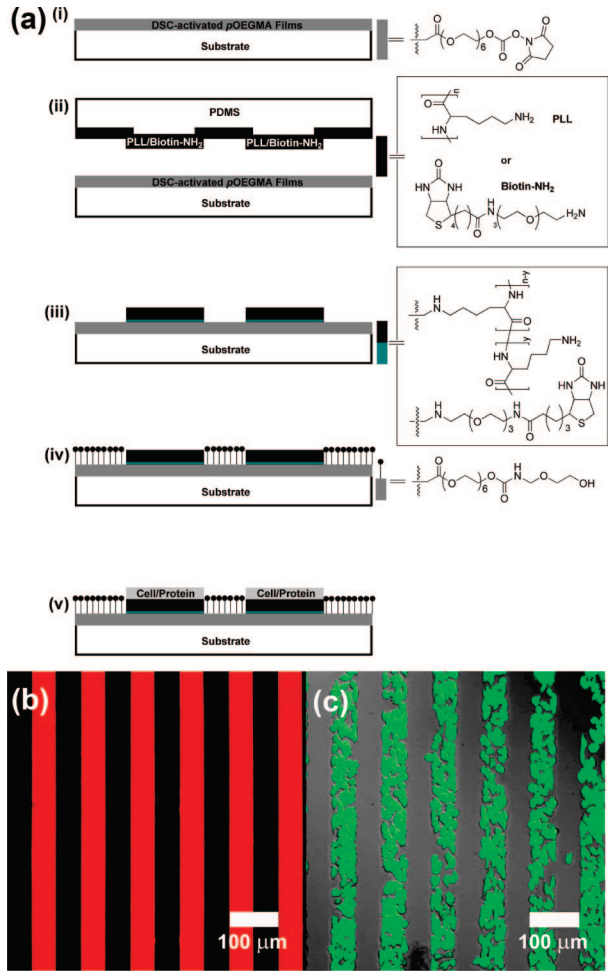

Figure 7. Pattern generation of proteins and cells. (a) Schematic representation of the procedure. Micropatterns of (b) streptavidin and (c) CHO-k1 cells.

the nonspecific binding of fibrinogen. The QCM frequency shift was 0.5 Hz on average with all the substrates, and any noticeable change was not observed by varying the thicknesses. The QCM frequency shift of 0.5 Hz corresponded to the mass change of 8.85 ng/cm^2, which was in the same order to the value obtained from the SPR studies (2.9 ng/cm^2). We believe that the difference in the absolute value was caused by the differences in the detection methods. In contrast, the binding capacity of SA was measured to be 29.6 (for 3 nm), 52.2 (for 8 nm), 63.5 (for 20 nm), 62.5 (for 31 nm), and 62 Hz (for 46 nm), which corresponded to 523.92, 923.94, 1123.95, 1106.25, and 1097.4 ng/cm^2, respectively. The QCM measurements indicated that the binding capacity (or the *S*/*N* ratio) was maximized and saturated at about 20 nm (Figure 6b, derived from Figure 6a). The increase of the binding capacity below the thickness of less than 20 nm could be rationalized by the increased number of functionalizable hydroxyl groups of polymer side chains. The saturation phenomenon of the binding capacity of SA over the 20 nm thickness was not clearly understood from the QCM measurements. Therefore, we calculated the thickness changes at each steps (DSC activation, biotin coupling, and SA adsorption) to get an insight into why the binding capacity of SA was saturated when the thickness was increased to more than 20 nm. We observed that the thickness change after the SA adsorption (a reference: biotin-presenting surfaces) was saturated earlier than those after the other two steps (DSC activation and biotin coupling) (Figure 6c). For example, the thickness change after the SA adsorption was saturated at about 26 nm, while that after biotin coupling was saturated at about 110 nm. The value of 26 nm was in agreement with the saturation value (20 nm) obtained by the QCM measurements. These results implies that the total number of biotin groups increased as the thicknesses of the *p*OEGMA films were increased, but the access of SA to some of biotin groups would be sterically screened. Therefore, the formation of thicker films over a critical thickness would not be optimal, and the consideration of the thickness should be made for maximizing binding specificity/capacity of biomolecules. Much work has been done to optimize the lateral surface density of probe molecules and the spaces between them.[24,52] The vertical effect of the bioplatform (vertical distribution of probe molecules) would be another important factor in the sensitivity of microarrays and biosensors.

Micropatterns of Proteins and Cells. Figure 7a showed a schematic representation of the procedure for patterning amine-terminated compounds onto the DSC-activated, 16 nm thick *p*OEGMA films. Briefly, the DSC-activated *p*OEGMA films were brought into a conformal contact with an oxidized PDMS stamp presenting micrometer-sized relief features, which had been inked with amine-terminated compounds. The pattern generation of biotin on the DSC-activated *p*OEGMA films was achieved by μCP of biotin-NH_2 with a PDMS stamp that had relief features with lateral dimensions of 50 μm (width of line). After patterning biotin-$NH_2$and passivating the remaining NHS carbonate ester groups with EG_2-NH_2, the samples were incubated in a PBS solution of rhodamin (TRITC)-conjugated

streptavidin. Successful patterning was verified by fluorescence microscopy (Figure 7b). To evaluate the feasibility of the *p*OEGMA-coated substrates for the selective cell attachment, PLL was also patterned onto the *p*OEGMA film by μCP for promoting cellular adhesion. Figure 7c shows the patterns of CHO-k1 cells after the deposition. The cells were confined only in the areas presenting PLL. In contrast, when cells were seeded onto the *p*OEGMA film, all the cells were detached from the substrate.

Conclusions

In summary, we fabricated biomolecule-functionalized *p*OEGMA films with various thicknesses with biotin as a model. Biotin was directly attached onto the activated *p*OEGMA films. The objectives of this work were (1) to develop a new method for directly functionalizing *p*OEGMA films as a bioconjugation platform, and (2) to investigate the effect of thickness of the *p*OEGMA films on the biospecific binding. The SPR data showed the enhanced binding specificity/capacity of the biotin-presenting *p*OEGMA films, compared with self-assembled monolayers (SAMs) and *p*OEGMEMA films. On the basis of the observed specificity/capacity, protein and cellular micropatterns were successfully generated. The QCM measurements indicated that the binding capacity of streptavidin was greatly affected by the thickness of the *p*OEGMA films and saturated at the 20 nm thick film. We believe that the method demonstrated herein is simple but versatile for generating semi-3-D, nonbiofouling polymer films. In addition, the SPR and QCM results implied that the thickness of the polymer films should be optimized for maximizing the biospecific binding of a target protein and the *S*/*N* ratios.

Acknowledgment. This work was supported by the Korea Science and Engineering Foundation Grant (R01-2005-000-10355-0) (ISC) and by the KBSI grant (N27072) (K-BL). We thank Dr. Mi-Sook Won at KBSI for the XPS analysis, Dr. Zee-Won Lee at KBSI for the confocal microscopy analysis, and Dr. Pil Sun Na and Jae-Hoon Jeong at Korea Bio-IT Foundry Center for the QCM measurements. FT-IR spectrophotometer and ellipsometer were purchased by a research fund from the Center for Molecular Design and Synthesis.

Supporting Information Available. QCM frequency shifts at various overtones ($n = 3$, 5, 7, 9, 11, and 13). This material is available free of charge via the Internet at http://pubs.acs.org.

References and Notes

(1) Leonard, E. F.; Turitto, V. T.; Vroman, L. *Blood in Contact with Natural and Artificial Surfaces*; New York Academy of Sciences: New York, 1987; Vol. 516.
(2) Gerhold, D.; Rushmore, T.; Caskey, C. T. *Trends Biochem. Sci.* **1999**, *24*, 168.
(3) Wilson, D. S.; Nock, S. *Angew. Chem., Int. Ed.* **2003**, *42*, 494.
(4) LaBaer, J.; Ramachandran, N. *Curr. Opin. Chem. Biol.* **2005**, *9*, 14.
(5) Uttamchandani, M.; Walsh, D. P.; Yao, S. Q.; Chang, Y.-T. *Curr. Opin. Chem. Biol.* **2005**, *9*, 4.
(6) Cretich, M.; Damin, F.; Pirri, G.; Chiari, M. *Biomol. Eng.* **2006**, *23*, 77.
(7) McArthur, S. L.; Mclean, K. M.; Kingshott, P.; St John, H. A. W.; Chatelier, R. C.; Griesser, H. J. *Colloids Surf. B* **2000**, *17*, 37.
(8) Österberg, E.; Bergström, K.; Holmberg, K.; Schuman, T. P.; Riggs, J. A.; Burns, N. L.; Van Alstine, J. M.; Harris, J. M. *J. Biomed. Mater. Res.* **1995**, *29*, 741.
(9) Kazuhiko, I.; Hideki, M.; Toshikazu, K.; Nobuo, N. *J. Biomed. Mater. Res.* **1995**, *29*, 181.
(10) Holmlin, R. E.; Chen, X.; Chapman, R. G.; Takayama, S.; Whitesides, G. M. *Langmuir* **2001**, *17*, 2841.
(11) Kane, R. S.; Deschatelets, P.; Whitesides, G. M. *Langmuir* **2003**, *19*, 2388.
(12) Chen, S.; Zheng, J.; Li, L.; Jiang, S. *J. Am. Chem. Soc.* **2005**, *127*, 14473.
(13) Chang, Y.; Chen, S.; Zhang, Z.; Jiang, S. *Langmuir* **2006**, *22*, 2222.
(14) Zhang, Z.; Chao, T.; Chen, S.; Jiang, S. *Langmuir* **2006**, *22*, 10072.
(15) Zhang, Z.; Chen, S.; Chang, Y.; Jiang, S. *J. Phys. Chem. B* **2006**, *110*, 10799.
(16) Cho, W. K.; Kong, B.; Choi, I. S. *Langmuir* **2007**, *23*, 5678.
(17) Prime, K. L.; Whitesides, G. M. *J. Am. Chem. Soc.* **1993**, *115*, 10714.
(18) Roberts, C.; Chen, C. S.; Mrksich, M.; Martichonok, V.; Ingber, D. E.; Whitesides, G. M. *J. Am. Chem. Soc.* **1998**, *120*, 6548.
(19) Lahiri, J.; Isaacs, L.; Tien, J.; Whitesides, G. M. *Anal. Chem.* **1999**, *71*, 777.
(20) Jon, S.; Seong, J.; Khademhosseini, A.; Tran, T.-N. T.; Laibinis, P. E.; Langer, R. *Langmuir* **2003**, *19*, 9989.
(21) Ghosh, P.; Amirpour, M. L.; Lackowski, W. M.; Pishko, M. V.; Crooks, R. M. *Angew. Chem., Int. Ed.* **1999**, *38*, 1592.
(22) Ma, H.; Hyun, J.; Stiller, P.; Chilkoti, A. *Adv. Mater.* **2004**, *16*, 338.
(23) Ma, H.; Li, D.; Sheng, X.; Zhao, B.; Chilkoti, A. *Langmuir* **2006**, *22*, 3751.
(24) Ma, H.; Wells, M., Jr.; Chilkoti, A. *Adv. Funct. Mater.* **2006**, *16*, 640.
(25) Tugulu, S.; Arnold, A.; Sielaff, I.; Johnsson, K.; Klok, H.-A. *Biomacromolecules* **2005**, *6*, 1602.
(26) Lee, B. S.; Lee, J. K.; Kim, W.-J.; Jung, Y. H.; Sim, S. J.; Lee, J.; Choi, I. S. *Biomacromolecules* **2007**, *8*, 744.
(27) Liu, V. A.; Jastromb, W. E.; Bhatia, S. N. *J. Biomed. Mater. Res.* **2002**, *60*, 126.
(28) Kidambi, S.; Chan, C.; Lee, I. *J. Am. Chem. Soc.* **2004**, *126*, 4697.
(29) Alcantar, N. A.; Aydil, E. S.; Israelachvili, J. N. *J. Biomed. Mater. Res.* **2000**, *51*, 343.
(30) Harris, J. M. *Poly(ethylene glycol) Chemistry: Biotechnical and Biomedical Applications*; Plenum Press: New York, 1992.
(31) Löfås, S. *Pure Appl. Chem.* **1995**, *67*, 829.
(32) Dai, J.; Bao, Z.; Sun, L.; Hong, S. U.; Baker, G. L.; Bruening, M. L. *Langmuir* **2006**, *22*, 4274.
(33) Sebra, R. P.; Masters, K. S.; Bowman, C. N.; Anseth, K. S. *Langmuir* **2005**, *21*, 10907.
(34) Raynor, J. E.; Petrie, T. A.; García, A. J.; Collard, D. M. *Adv. Mater.* **2007**, *19*, 1724.
(35) Shah, R. R.; Merreceyes, D.; Husemann, M.; Rees, I.; Abbott, N. L.; Hawker, C. J.; Hedrick, J. L. *Macromolecules* **2000**, *33*, 597.
(36) Azzaroni, O.; Moya, S.; Farhan, T.; Brown, A. A.; Huck, W. T. S. *Macromolecules* **2005**, *38*, 10192.
(37) Lee, J. K.; Kim, Y.-G.; Chi, Y. S.; Yun, W. S.; Choi, I. S. *J. Phys. Chem. B* **2004**, *108*, 7665.
(38) Böcking, T.; Kilian, K. A.; Hanley, T.; Ilyas, S.; Gaus, K.; Gal, M.; Gooding, J. J. *Langmuir* **2005**, *21*, 10522.
(39) Liedberg, B.; Lundström, I.; Stenberg, E. *Sens. Actuators, B* **1993**, *11*, 63.
(40) Vogt, B. D.; Lin, E. K.; Wu, W.-l.; White, C. C. *J. Phys. Chem. B* **2004**, *108*, 12685.
(41) Hamlin, R. E.; Dayton, T. L.; Johnson, L. E.; Johal, M. S. *Langmuir* **2007**, *23*, 4432.
(42) Kaufman, E. D.; Belyea, J.; Johnson, M. C.; Nicholson, Z. M.; Ricks, J. L.; Shah, P. K.; Bayless, M.; Pettersson, T.; Feldoto, Z.; Blomberg, E.; Claesson, P.; Franzen, S. *Langmuir* **2007**, *23*, 6053.
(43) Sauerbrey, G. Z. *Phys. Verh.* **1957**, *8*, 113.
(44) Sauerbrey, G. Z. *Z. Phys.* **1959**, *155*, 206.
(45) Lee, K.-B.; Kim, Y.; Choi, I. S. *Bull. Korean Chem. Soc.* **2003**, *24*, 161.
(46) Miura, Y.; Sato, H.; Ikeda, T.; Sugimura, H.; Takai, O.; Kobayashi, K. *Biomacromolecules* **2004**, *5*, 1708.
(47) Chi, Y. S.; Jung, Y. H.; Choi, I. S.; Kim, Y.-G. *Langmuir* **2005**, *21*, 4669.
(48) Homola, J.; Yee, S. S.; Gauglitz, G. *Sens. Actuators, B* **1999**, *54*, 3.
(49) Teare, D. O. H.; Schofield, W. C. E.; Garrod, R. P.; Badyl, J. P. S. *J. Phys. Chem. B* **2005**, *109*, 20923.
(50) Lukosz, W. *Biosens. Bioelectron.* **1997**, *12*, 175.
(51) Jung, L. S.; Campbell, C. T.; Chinowsky, T. M.; Mar, M. N.; Yee, S. S. *Langmuir* **1998**, *14*, 5636.
(52) Jones, D. M.; Brown, A. A.; Huck, W. T. S. *Langmuir* **2002**, *18*, 1265.

BM7009043